Electromagnetic Design of Microwave Cavities for Side-Coupled Linear Accelerators: A Hybrid Numerical/Analytical Approach

Dario Laneve, Mario Christian Falconi, *Student Member, IEEE*, Michele Bozzetti, Giovanni Rutigliani, Raffaele Andrea Prisco, Vincenzo Dimiccoli, and Francesco Prudenzano

***Abstract*— A homemade computer code for designing the coupled microwave cavities of a linear accelerator (linac) has been developed. A hybrid approach, based on both analytical investigation and numerical calculation, is exploited. A finite-element method (FEM) based on 2-D/3-D electromagnetic simulation software is used to find the eigenmodes and eigenfrequencies of the accelerator cavities as well as design typical figures of merit. The FEM investigation is integrated with a multiobjective particle swarm optimization approach in order to automatically optimize the geometry of the accelerating tanks. This approach seems very promising and general, allowing the optimization of a wide class of side-coupled resonant structures. The computer code is validated via measurements on a 27-MeV 3-GHz standing-wave side-coupled linac tank of five cavities closed with suitable end cells. The agreement between simulation and experiment is excellent; the displacement between the maxima of the simulated and measured longitudinal electric field modulus is close to 0.2%.**

***Index Terms*— Accelerator cavities, electromagnetic modeling, evolutionary optimization, linear accelerators (linacs), microwave devices, resonators.**

I. Introduction

MULTICAVITY structures are employed for both electromagnetic field coupling and particle beam acceleration or spatial/velocity beam modulation in a number of applications including high-power microwave sources, relativistic klystron amplifiers, microwave rebuncher cavities, microwave plasma sources, novel sheet-beam klystrons, magnetron combining, and linear particle accelerators (linacs) [1]–[13]. In such applications, the number of geometrical parameters to be optimized is very high (dozens of parameters) [14]. Moreover, in the design of side-coupled linacs (SCLs), accurate electromagnetic simulations must be performed in order to obtain the identity (or closeness) of the modal resonant frequencies of the following: i) the overall linac stages (tanks); ii) the coupling cavities (CCs) and iii) the accelerating cavities (ACs) loaded by mutual coupling effects, to minimize the SCL stopband [14]. Another important design goal is iv) the electromagnetic field uniformity along the accelerating structure, i.e. the invariance of the longitudinal electric field modulus along the tank cavities.

Many commercial codes provide internal tools to minimize/maximize particular figures of merit via global methods, such as the artificial neural networks, the genetic algorithms, and the particle swarm optimization (PSO) approach [15]–[19]. Despite this, the objectives 1)–4) cannot be simultaneously taken into account and carried out by employing the internal tools of the commercial codes. In these cases, a number of simulations are needed via trial and error approach. We underline that the main strength of the proposed approach is the partial automation of the design procedure. From our experience with commercial codes, the complex design procedure causes downtime between consecutive simulations due to the need for decision making in order to define the new optimization trials. The wasted time is thus not eliminable by using just more powerful computational resources.

In this paper, a novel hybrid approach (HA) implemented via a homemade computer code integrating a full 3-D numerical investigation with an analytical (in closed-form expression) model approximating the periodic structure of an SCL is proposed. A multiobjective PSO (MOPSO) approach is employed for the global solution search [20]. This allows an extremely efficient and fully automated design. The homemade computer code is employed for designing a 27-MeV 3-GHz standing-wave SCL tank of 35 cavities for hadrontherapy applications [12]. To investigate the feasibility of this SCL tank, a shorter tank consisting of five cavities closed with suitable end cells (ECs) is designed and fabricated; to this aim, the spatial period of the tank of five cavities is the same as that considered for the tank of 35 cavities. In addition, the characterization of the fabricated five-cavity tank allows validating the proposed HA. An excellent agreement between simulation and experiment is obtained. The code is very efficient and can be employed for the design of a wide class of resonant structures.

Manuscript received May 21, 2018; accepted June 23, 2018. Date of publication June 28, 2018; date of current version August 15, 2018. This work was supported in part by the Ministero dello Sviluppo Economico through the research project "ERHA—Enhanced Radiotherapy with Hadron," Horizon 2020, n. F/050425/02/X32 under Grant PON I&C 2014-2020, and in part by EU COST Action under Grant MP1401. *(Corresponding author: Francesco Prudenzano.)*

D. Laneve, M. C. Falconi, M. Bozzetti, and F. Prudenzano are with the Department of Electrical and Information Engineering, Polytechnic University of Bari, 70126 Bari, Italy (e-mail: dario.laneve@poliba.it; mariochristian.falconi@poliba.it; michele.bozzetti@poliba.it; francesco.prudenzano@poliba.it).

G. Rutigliani, R. A. Prisco, and V. Dimiccoli are with ITEL Telecomunicazioni S.r.l., 70037 Bari, Italy (e-mail: g.rutigliani@itelte.it; r.prisco@itelte.it; v.dimiccoli@itelte.it).

Color versions of one or more of the figures in this paper are available online at http://ieeexplore.ieee.org.

Digital Object Identifier 10.1109/TNS.2018.2851387

II. HYBRID APPROACH

The MOPSO algorithm [20] is used to find the optimal geometry of the linac cavities with respect to the design specifications, or objectives, which will be described in the following. The homemade code relies on a hybrid analytical/numerical approach. The 3-D numerical investigation is based on a commercial finite-element method (FEM) software integrated with the MOPSO routine. An initial geometry is defined in the 3-D FEM interface, starting from geometrical parameters inspired by [21]. For each tentative solution (set of tentative geometrical parameters), the homemade code drives the 3-D FEM simulation:

1) the resonant modes of the whole tank are calculated via FEM investigations;
2) the analytical dispersion equation is calculated at each modal frequency [14];
3) thus, an equation system is written and solved [22].

The coupling coefficients and the loaded resonant frequencies of the tentative ACs and CCs are the solutions of the abovementioned equation system [22]. This step is very fast due to the closed-form expressions. Then, the multiobjective function is calculated along with the constraints of the optimization problem. The MOPSO routine allows finding the best global solutions by exploiting the Pareto optimality condition [23]. The electromagnetic field uniformity is then obtained via a further refinement procedure in few steps. To the best of our knowledge, this hybrid strategy is applied for the first time, via the homemade computer code, to obtain a completely automated electromagnetic design of linac cavities, not allowed by commercial codes. Moreover, a strong reduction of calculation time is achieved, by our experience 2/3 times shorter if compared with the nonautomated conventional design procedures. In the following, for ease of reading, the homemade computer code will be named as HA.

We consider the complex microwave SCL cavities of Fig. 1, in which a number of fillets and protrusions are included to improve the acceleration efficiency, increase the quality factor, and modulate the resonant frequency. These kinds of geometries are largely employed in linacs [21], [22] similar to that employed in ITEL plant [24]. A list of the geometrical parameters of the cavities is given in Tables I and II (see first two columns).

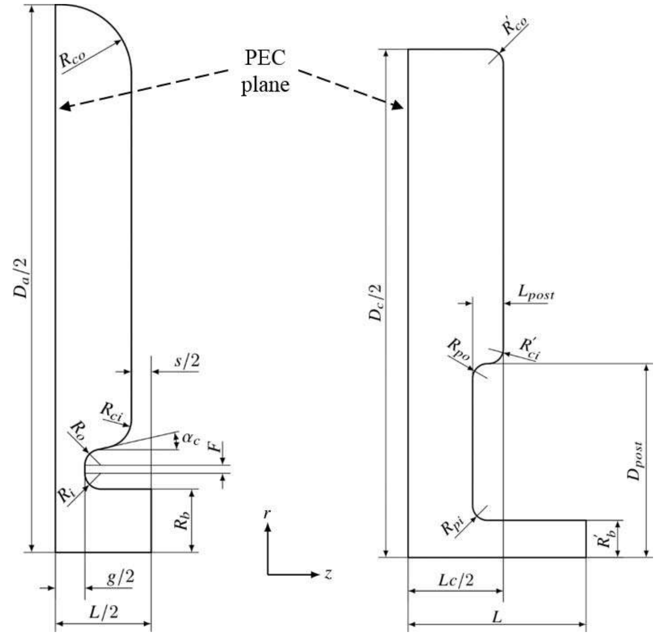

(a) (b)

Fig. 1. Sketches of the (a) AC and (b) CC half cells, along with their design geometrical parameters listed in Tables I and II. Both cells are axisymmetric around the z-axis.

TABLE I
OPTIMIZED GEOMETRICAL PARAMETERS OF ACs AND CCs

Parameter	Description	Search space (mm)[a]	Optimized value (mm)[a]
D_a	ACs diameter	[50.0, 75.0]	67.125
g	ACs gap length	[1.0, 5.0]	3.059
R_{co}	ACs outer corner radius	[3.4, 10.0]	3.875
F	ACs flat length	[0.0, 2.0]	0.718
α_c	ACs cone angle	[0.0, 20.0]°	6.686°
s	ACs septum thickness	[1.2, 4.0]	2.890
L_c	CCs length	[5.0, 15.0]	11.550
D_c	CCs diameter	[50.0, 75.0]	68.469
L_{post}	CCs post length	[2.0, 6.0]	2.559
D_{post}	CCs post diameter	[10.0, 50.0]	18.061
Interaxis	Distance between ACs and CCs longitudinal axes	[62.0, 72.0]	63.848

[a]Except α_c.

III. ANALYTICAL MODEL

The frequency of a peculiar propagation mode of the SCL is related to the phase advance of the electromagnetic field per accelerating period according to the following dispersion relation [14]:

$$k_1^2\cos^2\phi = \left(1 - \frac{\omega_a^2}{\omega_q^2} + k_a\cos 2\phi\right)\left(1 - \frac{\omega_c^2}{\omega_q^2} + k_c\cos 2\phi\right) \quad (1)$$

where $\phi = \pi q/2N$, $q = 0, 1, \ldots, 2N$, is the phase advance per period of the $(q+1)$th propagating mode at the frequency ω_q, N is the number of CCs, and $N+1$ is the number of ACs; ω_a and ω_c are the frequencies of ACs and CCs, respectively; k_1 is the coupling constant between ACs and CCs; k_a and k_c are the coupling constants between adjacent ACs and adjacent CCs, respectively [14]. For the $\pi/2$ mode $(q = N)$, the dispersion relation has two solutions $\omega_{\pi/2,\text{AC}} = \omega_a/(1-k_a)^{1/2}$ depending on the chain of the coupled ACs and $\omega_{\pi/2,CC} = \omega_c/(1-k_c)^{1/2}$ depending on the chain of the coupled CCs. The difference between these frequency solutions is the so-called stopband [14]. For a good design and a proper operation of the SCL, the stopband must be as small as possible, i.e., the cavities must be geometrically refined and tuned such that $\omega_{\pi/2,\text{AC}} = \omega_{\pi/2,CC}$.

A tank of five cavities, or quintuplet, closed with half CCs is considered. It is illustrated in Fig. 2. According to the image theory [25], a finite-length SCL tank closed with half CCs has

TABLE II
CONSTANT GEOMETRICAL PARAMETERS OF ACs AND CCs

Parameter	Description	Value (mm)
L	Cell length (period)	12.140
R_{ci}	ACs inner corner radius	1.8
R_i	ACs inner nose radius	1.0
R_o	ACs outer nose radius	1.0
R_b	ACs bore radius	4.0
R'_{co}	CCs outer corner radius	1.0
R'_{ci}	CCs inner corner radius	1.0
R_{pi}	CCs inner post radius	1.0
R_{po}	CCs outer post radius	1.0
R'_b	CCs bore radius	2.5

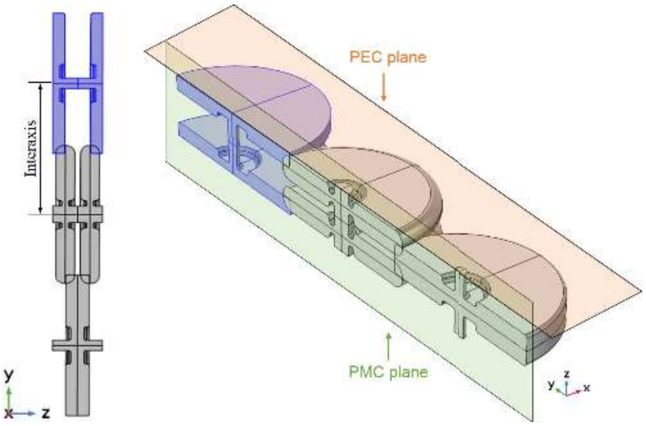

(a) (b)

Fig. 2. (a) Cross section of the SCL tank of five cavities (two ACs and three CCs) closed with half CCs (highlighted in blue). (b) 3-D view of the tank. The bottom PEC plane is not shown.

the same electromagnetic field distribution of an infinitely long SCL tank [22]. The five electromagnetic parameters, ω_a, ω_c, k_a, k_c, and k_1, are calculated by substituting in (1) the frequencies ω_q, $q = 0, \ldots, 4$, of the five eigenmodes simulated via FEM. The following system of five equations is thus obtained:

$$\begin{cases} k_1^2 = \left(1 - \dfrac{\omega_a^2}{\omega_0^2} + k_a\right)\left(1 - \dfrac{\omega_c^2}{\omega_0^2} + k_c\right) & q = 0 \\ \dfrac{k_1^2}{2} = \left(1 - \dfrac{\omega_a^2}{\omega_1^2}\right)\left(1 - \dfrac{\omega_c^2}{\omega_1^2}\right) & q = 1 \\ 0 = \left(1 - \dfrac{\omega_a^2}{\omega_2^2} - k_a\right)\left(1 - \dfrac{\omega_c^2}{\omega_2^2} - k_c\right) & q = 2 \\ \dfrac{k_1^2}{2} = \left(1 - \dfrac{\omega_a^2}{\omega_3^2}\right)\left(1 - \dfrac{\omega_c^2}{\omega_3^2}\right) & q = 3 \\ k_1^2 = \left(1 - \dfrac{\omega_a^2}{\omega_4^2} + k_a\right)\left(1 - \dfrac{\omega_c^2}{\omega_4^2} + k_c\right) & q = 4. \end{cases} \tag{2}$$

By solving this polynomial equation system, ω_a, ω_c, k_a, k_c, and k_1 are obtained. The frequency of the $\pi/2$ mode is then calculated as $\omega_{\pi/2} = \omega_2 = \omega_c/(1 - k_c)^{1/2}$.

TABLE III
MOPSO SETTINGS

Parameter	Description	Value
N_{pop}	Number of particles (population size)	50
N_{iter}	Number of iterations	100
c_1	Cognitive constant	1
c_2	Social constant	1
w	Inertia weight	0.4
N_{grid}	Number of divisions of the adaptive grid	30
N_{rep}	Repository size	50
M	Mutation rate	0.5

IV. HYBRID APPROACH CODE DETAILS

The HA computer code, by exploiting FEM numerical simulations, realistically models both ACs and CCs. The following components of the biobjective vector-valued function $\boldsymbol{F}(\boldsymbol{x}) = [f_1(\boldsymbol{x}), f_2(\boldsymbol{x})]$ are simultaneously minimized:

$$f_1(\boldsymbol{x}) = |\omega_a(\boldsymbol{x})/\sqrt{1 - k_a(\boldsymbol{x})} - \omega_{\pi/2,\text{ref}}| \tag{3}$$

$$f_2(\boldsymbol{x}) = |\omega_c(\boldsymbol{x})/\sqrt{1 - k_c(\boldsymbol{x})} - \omega_{\pi/2,\text{ref}}| \tag{4}$$

where the vector $\boldsymbol{x}$ contains the geometrical parameters to be optimized, as listed in Table I; $\omega_{\pi/2,\text{ref}}$ is the reference value of the linac resonant frequency, as given by the design specifications (Section V). The simultaneous minimization of the two objective components, $f_1(\boldsymbol{x})$ and $f_2(\boldsymbol{x})$, ensures that the two frequency solutions of the $\pi/2$ mode, $\omega_{\pi/2,\text{AC}}(\boldsymbol{x})$ and $\omega_{\pi/2,CC}(\boldsymbol{x})$, tend to $\omega_{\pi/2,\text{ref}}$. As a consequence, the difference between the two objectives, i.e., the stopband, tends to zero. Moreover, a suitable constraint $k_{1,\min} \leq k_1 \leq k_{1,\max}$ is imposed on the optimization problem to increase the frequency separation between the $\pi/2$ mode and the adjacent modes, without increasing the power losses [14]. Finally, in the last part of the design (Section V-B), the uniformity of the accelerating field is taken into account. In particular, to ensure that protons gain about the same amount of energy in each accelerating cavity, the relative standard deviation, σ_R, of the longitudinal electric field peaks is kept below a fixed threshold $\sigma_{R,\max}$. The details on all the design criteria/constraints are illustrated in Section V.

The HA code is organized as follows. After reading the settings of the MOPSO routine, described in Table III, the positions and velocities of the swarm particles are initialized. The Pareto-optimal solutions, found during the search process, are stored in a repository and updated at each iteration. At the end of the procedure, this repository contains the solutions representing the best tradeoffs between the design goals. By exploiting the fitness sharing technique and the mutation operator [20], the HA code preserves the population diversity, avoiding the concentration of tentative solutions in a narrow portion of the objective space. The HA code iterates over the following steps until the convergence criterion is met:

1) select the global best position, i.e., the leader of the swarm;
2) update the position and the velocity of each particle;
3) apply the mutation operator to the particles;
4) simulate via FEM the AC and CC half cells to identify their unloaded frequencies, i.e., the frequencies with

TABLE IV

DESIGN PARAMETERS USED TO COMPUTE THE CELL LENGTH

Parameter	Description	Value
n_{ACs}	Number of ACs	18
$f_{\pi/2,\mathrm{ref}}$	Nominal frequency of π/2 mode (MHz)	2997.92
E_{in}	Input energy of the proton beam (MeV)	27
E_0	Mean accelerating electric field (MV/m)	15
T	Nominal transit-time factor	0.80
ϕ_s	Phase of the reference particle (°)	-20

no couplings, and calculate the following figures of merit: Q factor, power losses, transit-time factor, (effective) shunt impedance, peak surface electric field, bravery factor, and the so-called r over Q [14];

5) simulate via FEM the quintuplet with half CC terminations;
6) analytically calculate the loaded frequencies of ACs and CCs, ω_a and ω_c, and the coupling constants k_1, k_a, and k_c, by solving the polynomial equation system in (2);
7) evaluate the multiobjective function $\boldsymbol{F}(\boldsymbol{x})$ according to (3) and (4);
8) update the repository with the new Pareto-optimal solutions [20].

The code stops when the convergence criterion is met; then, it returns the optimized tank geometry.

V. DESIGN

The electromagnetic design of an SCL tank consisting of 35 cavities, 18 ACs, and 17 CCs is performed via the HA computer code. The cell length, L, i.e., the spatial period of the tank, is fixed by taking into account the following:

1) the desired number of ACs, n_{ACs};
2) the reference linac frequency, $f_{\pi/2,\mathrm{ref}}$ $(= \omega_{\pi/2,\mathrm{ref}}/2\pi)$;
3) the proton input energy, E_{in};
4) the mean accelerating electric field, E_0;
5) realistic value of the transit-time factor, T [21], [22];
6) realistic phase of the reference particle, ϕ_s [21], [22].

All these quantities are listed in Table IV, and the calculated cell length is listed in Table II. Moreover, the values $k_{1,\min} = 3\%$ and $k_{1,\max} = 4\%$ are considered for the constraint imposed on $\boldsymbol{F}(\boldsymbol{x})$, according to [21], [22]. Finally, to maximize the longitudinal electric field uniformity, the relative standard deviation of the field peaks is kept below $\sigma_{R,\max} = 3\%$. The set of these parameters, in addition to the stopband minimization, represents the design specifications.

A. Accelerating and Coupling Cavities' Optimization

Table I lists the design geometrical parameters of both ACs and CCs, the search ranges, and the Pareto-optimized parameters (global solution). The search ranges are set large enough to provide swarm with very good exploratory capabilities and they are consistent with the literature [21], [22], as well as the parameters kept constant during the optimization process (Table II). In particular, the radius of the aperture between adjacent ACs R_b is set to a value providing the high

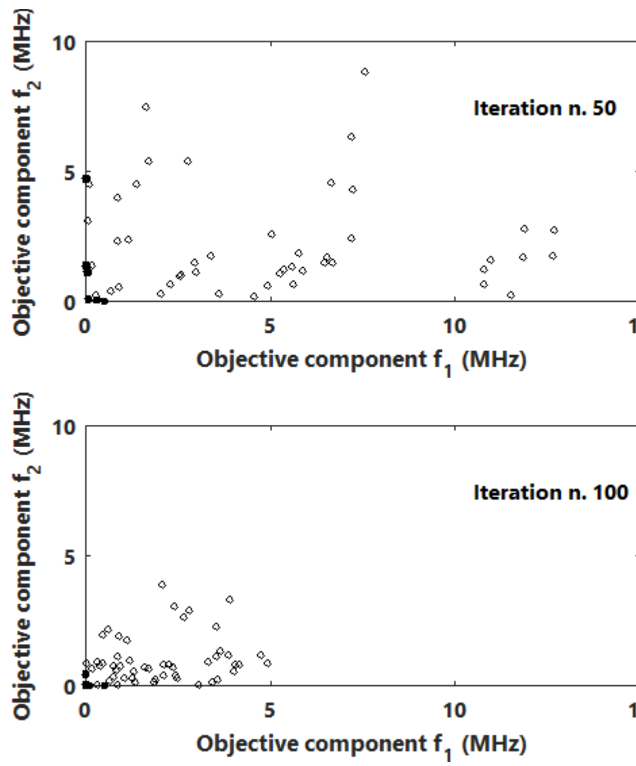

Fig. 3. Convergence of particles in the objective space at different iteration numbers. The objective components, f_1 and f_2, are given in (3) and (4).

transmittance of the beam. The settings of the MOPSO routine are listed in Table III. The values of c_1, c_2, w, N_{grid}, and M are those suggested in [20]. The values of N_{pop}, N_{iter}, and N_{rep} are chosen with the aim of reducing the computational cost of the approach, while maintaining a good population diversity and ensuring accurate results. Moreover, the invisible boundary condition is imposed on the search space [16]. However, the computation time mainly depends on the mesh settings defined for 3-D simulations, particularly on the smallest mesh size. For the smallest mesh size of 1 mm and the settings listed in Table III, the HA tank design requires about a week with a PC with an Intel Core i7-4770 and 16 GB of RAM. Reducing the computational effort is not trivial. A possible solution is to avoid 3-D simulations by estimating the coupling constants through known analytical formulas [26], [27]. Other solutions are as follows:

1) using coarser meshes;
2) using smaller search ranges and lowering the number of swarm particles;
3) lowering the number of iterations;
4) simulating a triplet, rather than a quintuplet, at each iteration, by neglecting k_a and k_c (especially at higher energies);
5) optimizing the code to exploit the modern multi-core/multiprocessor computer architectures.

All these solutions, with the exception of 5), can affect the simulation accuracy, and a tradeoff is required.

Fig. 3 illustrates the convergence of the particle swarm in the objective space at the 50th and 100th iterations. The full circles represent the Pareto-optimal points collected in

TABLE V
FREQUENCIES AND COUPLING CONSTANTS OF THE OPTIMIZED SCL CAVITIES

Parameter	Description	Value
f_a	Frequency of ACs (MHz)	3007.145
f_c	Frequency of CCs (MHz)	2997.866
k_a	Coupling constant between adjacent ACs	-6.03×10^{-3}
k_c	Coupling constant between adjacent CCs	1.80×10^{-4}
k_1	Coupling constant between ACs and CCs	3.23×10^{-2}

the repository up to the considered iteration, while the empty circles represent the actual population. The coordinate axes are those given by (3) and (4). The solutions tend to reside near the origin of the objective space. Since the coordinate axes are exactly f_1 and f_2, this means that the solutions are those for which $\omega_{\pi/2,\mathrm{AC}} \cong \omega_{\pi/2,\mathrm{ref}}$ and $\omega_{\pi/2,CC} \cong \omega_{\pi/2,\mathrm{ref}}$, so the stopband approximately equals zero. Then, the best global solution selected from the repository is the particle with the smallest stopband (less than 1 MHz).

Table V lists the frequencies and coupling constants of the optimized cavities. The corresponding stopband is very small, being about 12.5 kHz. The simulated values of the unloaded Q factor Q_0 and effective shunt impedance per unit length ZT^2 of the ACs are $Q_0 = 6180$ and $ZT^2 = 30.9$ MΩ/m, respectively.

B. End Cells and Tank Simulations

The results illustrated in Section V-A, by considering the tank as an infinite periodic structure, are propaedeutic for a realistic linac design. Different boundary conditions are taken into account in this section, since in actual plants the tanks are closed with full ACs. The resonant frequency of these closing ACs is related to the results illustrated in Section V-A.

The symmetry of the $\pi/2$ mode of the SCL is preserved if both the closing ACs, also known as ECs, are modified so that their resonant frequency is equal to [21]

$$f_{\mathrm{EC}} = f_a \sqrt{\frac{1 - k_a/2}{1 - k_a}}. \quad (5)$$

The ECs frequency, f_{EC}, depends on frequency f_a $(= \omega_a/2\pi)$, of the intermediate ACs and the coupling constant k_a between adjacent ACs. Both these quantities are listed in Table V. The calculated frequency of the ECs is $f_{\mathrm{EC}} = 3002.637$ MHz.

To validate the HA computer code, a shorter tank of five optimized cavities (see Table I) is considered. It consists of two ECs, one central ACs and two side CCs, as illustrated in Fig. 4. In the design, starting from the optimized ACs, the two ECs are then finely tuned so that: 1) the relative standard deviation of the maxima of the longitudinal electric field modulus along the beam axis, $|E_z|$, is less than $\sigma_{R,\max} = 3\%$ and 2) the frequency of the $\pi/2$ mode is equal to $\omega_{\pi/2,\mathrm{ref}}$. To this aim, the gap and the nose flat length of just the outer halves of the ECs are varied (see Fig. 4). Following this tuning step, the small value $\sigma_{R,\mathrm{sim}} = 1.806\%$ is obtained and the frequency of the $\pi/2$ mode is $f_{\pi/2,\mathrm{sim}} = 2997.916$ MHz, practically coincident with $f_{\pi/2,\mathrm{ref}}$.

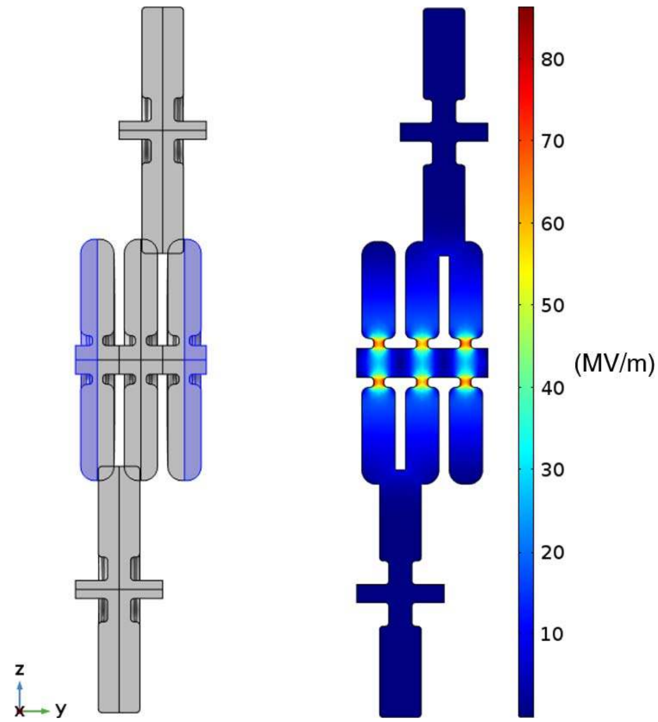

(a) (b)

Fig. 4. Fabricated five-cavity tank with EC terminations. (a) Geometry optimized with the HA computer code; the outer halves of the two ECs are highlighted in blue. (b) Simulated electric field norm of the $\pi/2$ mode.

In Fig. 4, the electric field norm distribution of the resonating $\pi/2$ mode is illustrated. As expected, the field is mainly confined in the ACs, near the beam axis, and it is negligible in the CCs.

VI. MEASUREMENTS

The five-cavity tank closed with the ECs of Fig. 4 is fabricated and characterized. The high purity oxygen-free electronic grade copper is used to fabricate the cavities. The plates used to assemble the cavities are held together by means of clamps. No brazing process is adopted, and the quality factor is not measured. The five eigenfrequencies of the fabricated tank are measured by means of a vector network analyzer (VNA Anritsu MS4644B): $f_0 = 2959.719$ MHz, $f_1 = 2972.545$ MHz, $f_2 = f_{\pi/2,\mathrm{meas}} = 2997.796$ MHz, $f_3 = 3025.050$ MHz, and $f_4 = 3049.900$ MHz. The longitudinal electric field amplitude is measured by means of the same VNA. According to the standard bead-perturbation measurement technique [28], a small cylindrical bead is moved through the cavities by a thin nylon line attached to a stepper motor. The motor, in turn, is connected to a digital-analog converter for PC control. The RF excitation is provided to the cavities by two magnetic probes (loop antennas), located into the first and last ACs. The S_{12} scattering parameter is measured through the VNA. In particular, a reference attenuation level of −45 dB is chosen. The estimated frequency shift due to the field probes is negligible (about 100 kHz). The driving frequency of the VNA is locked to the resonant frequency of the $\pi/2$ mode. The measured frequency is $f_{\pi/2,\mathrm{meas}} = 2997.796$ MHz in excellent agreement with the simulated one.

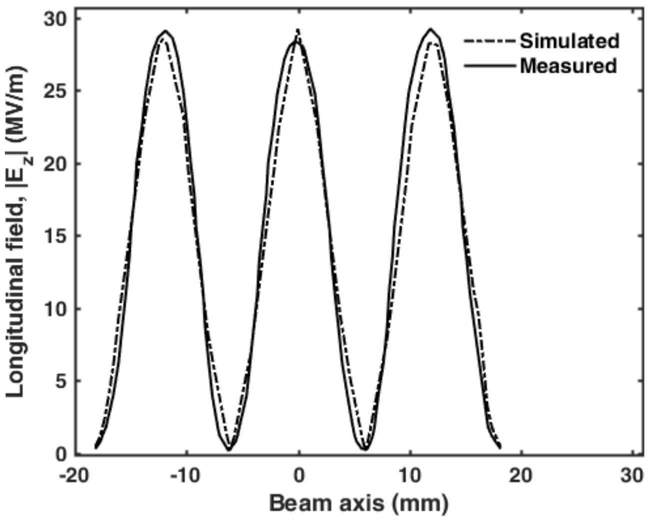

Fig. 5. Comparison between the simulated and measured longitudinal component of the electric field along the tank cavities.

According to the Slater theorem [14], the bead-induced cavity frequency shift is proportional to the square of the local field. In this way, the electric field amplitude is measured in each accelerating gap. The beam pipe-like structure in the CCs is used for the bead-perturbation measurement of the electric field in the CCs. As expected from the simulation, see Fig. 4, negligible values of the electric field in the CCs have been measured. The beam pipe-like structure in the CCs can be removed from the final design. The cavities are tuned via metallic rods to maximize the field uniformity. The rods are located at the center of the cylindrical wall of each cavity. The rods slightly affect the resonant frequency of the $\pi/2$ mode by inducing a shift of about ±150 kHz. This shift can be compensated through a temperature increase/decrease of about 3 °C. In Fig. 5, the simulated and measured longitudinal electric field modulus, $|E_z|$, are shown for comparison. The two curves are normalized to have the mean accelerating field $E_0 = 15$ MV/m along the beam axis, which is equivalent to a simulated peak input power of about $P_{\text{in}} = 200$ kW. Fig. 5 shows an excellent agreement; the displacement between the maxima of the simulated and measured longitudinal electric field modulus $|E_z|$ is close to 0.2%. In fact, the measured field uniformity is $\sigma_{R,\text{meas}} = 1.585\%$, practically coincident with the simulated one. The differences between the simulated and measured values of E_z may be due to the fabrication tolerances and/or to the small differences between the E_z measurement points and the simulation nodes.

We underline that the proposed approach can be efficiently applied to the design of longer tanks, typically employed in actual linacs, allowing larger reduction of computation cost and strongly helping the design work. Moreover, it is very versatile and can be used for the design of other complex resonating structures.

VII. Conclusion

A powerful computer code is written in order to design the complex resonant cavities of an SCL. An FEM is integrated with both the MOPSO approach and an analytical investigation. The proposed hybrid strategy allows performing an automated design. The goodness of the proposed approach is confirmed via the experimental validation on a short, five-cavity, tank prototype. As an example, the simulated and the measured resonant frequency of the designed SCL five-cavity tank are $f_{\pi/2,\text{sim}} = 2997.916$ MHz and $f_{\pi/2,\text{meas}} = 2997.796$ MHz, respectively. Moreover, the measured field uniformity is $\sigma_{R,\text{meas}} = 1.585\%$, only 0.2% smaller than the simulated one. This approach is very promising and general; it can be applied to the optimization of a larger number of figures of merit concerning the linac cavities, such as the Q-factor, the shunt impedance, and the ratio E_s/E_0; E_s is the peak surface electric field. Moreover, the described approach can be applied to the design of a wide class of resonating multicavity structures for different applications.

References

[1] D. Zhao, X. Lu, Y. Liang, X. Yang, C. Ruan, and Y. Ding, "Researches on an X-band sheet beam klystron," *IEEE Trans. Electron Devices*, vol. 61, no. 1, pp. 151–158, Jan. 2014.

[2] Y.-M. Shin, L. R. Barnett, and N. C. Luhmann, "Quasi-optical output-cavity design for a 50-kW multicavity W-band sheet-beam klystron," *IEEE Trans. Electron Devices*, vol. 56, no. 12, pp. 3196–3202, Dec. 2009.

[3] Y.-M. Shin, J.-X. Wang, L. R. Barnett, and N. C. Luhmann, "Particle-in-cell simulation analysis of a multicavity W-band sheet beam klystron," *IEEE Trans. Electron Devices*, vol. 58, no. 1, pp. 251–258, Jan. 2011.

[4] M. E. Read, V. Jabotinski, G. Miram, and L. Ives, "Design of a gridded gun and PPM-focusing structure for a high-power sheet electron beam," *IEEE Trans. Plasma Sci.*, vol. 33, no. 2, pp. 647–653, Apr. 2005.

[5] K. W. Lee, J. G. Jeong, Y. J. Yoon, J. H. Kim, and C. Kook, "Analysis of the quality factor of input cavity with intense beam loading in a relativistic vacuum tube," *IET Sci., Meas. Technol.*, vol. 11, no. 2, pp. 141–148, Mar. 2017.

[6] H. Nowakowska, M. Jasinski, P. S. Debicki, and J. Mizeraczyk, "Numerical analysis and optimization of power coupling efficiency in waveguide-based microwave plasma source," *IEEE Trans. Plasma Sci.*, vol. 39, no. 10, pp. 1935–1942, Oct. 2011.

[7] Y. Wu, Z. Xu, X. Jin, Z.-H. Li, and C.-X. Tang, "A long pulse relativistic klystron amplifier driven by low RF power," *IEEE Trans. Plasma Sci.*, vol. 40, no. 10, pp. 2762–2766, Oct. 2012.

[8] K. R. Shin, Y. W. Kang, and A. E. Fathy, "Design guidelines of a double-gap microwave rebuncher cavity for a 400 MHz, 2.5 MeV energy light ion accelerator with lower gap voltage and field," *IEEE Trans. Nucl. Sci.*, vol. 61, no. 2, pp. 817–823, Apr. 2014.

[9] Y. Zhang, K. Huang, D. K. Agrawal, T. Slawecki, H. Zhu, and Y. Yang, "Microwave power system based on a combination of two magnetrons," *IEEE Trans. Electron Devices*, vol. 64, no. 10, pp. 4272–4278, Oct. 2017.

[10] E. A. Knapp, "Resonantly coupled standing wave accelerator structures for electron and proton linac applications," *IEEE Trans. Nucl. Sci.*, vol. NS-16, no. 3, pp. 329–337, Jun. 1969.

[11] U. Amaldi *et al.*, "LIBO—A linac-booster for protontherapy: Construction and tests of a prototype," *Nucl. Instrum. Methods Phys. Res. A, Accel. Spectrom. Detect. Assoc. Equip.*, vol. 521, nos. 2–3, pp. 512–529, 2004.

[12] U. Amaldi *et al.*, "Accelerators for hadrontherapy: From Lawrence cyclotrons to linacs," *Nucl. Instrum. Methods Phys. Res. A, Accel. Spectrom. Detect. Assoc. Equip.*, vol. 620, nos. 2–3, pp. 563–577, 2010.

[13] S. Benedetti, A. Grudiev, and A. Latina, "High gradient linac for proton therapy," *Phys. Rev. Accel. Beams*, vol. 20, no. 4, p. 040101, Apr. 2017.

[14] T. P. Wangler, *RF Linear Accelerators*, 2nd ed. Weinheim, Germany: Wiley, 2008.

[15] J. Kennedy and R. C. Eberhart, *Swarm Intelligence*. San Francisco, CA, USA: Morgan Kaufmann, 2001.

[16] J. Robinson and Y. Rahmat-Samii, "Particle swarm optimization in electromagnetics," *IEEE Trans. Antennas Propag.*, vol. 52, no. 2, pp. 397–407, Feb. 2004.

[17] M. C. Falconi *et al.*, “Dysprosium-doped chalcogenide master oscillator power amplifier (MOPA) for Mid-IR emission,” *J. Lightw. Technol.*, vol. 35, no. 2, pp. 265–273, Jan. 15, 2017.

[18] G. Palma *et al.*, “Design of praseodymium-doped chalcogenide micro-disk emitting at 4.7 μm,” *Opt. Express*, vol. 25, no. 6, pp. 7014–7030, 2017.

[19] S. Dehuri, A. K. Jagadev, and M. Panda, Eds., *Multi-objective Swarm Intelligence*. Berlin, Germany: Springer-Verlag, 2009.

[20] C. A. Coello Coello, G. T. Pulido, and M. S. Lechuga, “Handling multiple objectives with particle swarm optimization,” *IEEE Trans. Evol. Comput.*, vol. 8, no. 3, pp. 256–279, Jun. 2004.

[21] L. Picardi, C. Ronsivalle, and A. Vignati, “Progetto del TOP LINAC,” ENEA Res. Centre, Frascati, Italy, Tech. Rep. RT/INN/97/17, Jul. 1997.

[22] U. Amaldi, S. Braccini, and P. Puggioni, “High frequency linacs for hadrontherapy,” *Rev. Accel. Sci. Technol.*, vol. 2, no. 1, pp. 111–131, 2009.

[23] C. A. Coello Coello, G. B. Lamont, and D. A. van Veldhuizen, *Evolutionary Algorithms for Solving Multi-Objective Problems*, 2nd ed. New York, NY, USA: Springer, 2007.

[24] *ERHA (Enhanced Radiotherapy with HAdrons)*. Accessed: Mar. 14, 2018. [Online]. Available: http://www.itelte.it/it/cnt/erha

[25] C. A. Balanis, *Advanced Engineering Electromagnetics*, 2nd ed. Hoboken, NJ, USA: Wiley, 2012.

[26] J. Gao, “Analytical formulas for the resonant frequency changes due to opening apertures on cavity walls,” *Nucl. Instrum. Methods Phys. Res. A, Accel. Spectrom. Detect. Assoc. Equip.*, vol. 311, no. 3, pp. 437–443, 1992.

[27] R. Roy and O. Shanker, “Calculation of intercavity coupling coefficient for side coupled standing wave linear accelerator,” *IEEE Trans. Microw. Theory Techn.*, vol. 41, no. 6, pp. 1233–1235, Jun. 1993.

[28] L. C. Maier, Jr., and J. C. Slater, “Field strength measurements in resonant cavities,” *J. Appl. Phys.*, vol. 23, no. 1, pp. 68–77, 1952.